Density functional study on the electronic and molecular structure of the hydroformylation catalyst HCo(CO)3

Tom Ziegler, Luigi Cavallo, and Attila Berces

Organometallics, **1993**, 12 (9), 3586-3593• DOI: 10.1021/om00033a034 • Publication Date (Web): 01 May 2002

Density Functional Study on the Electronic and Molecular Structure of the Hydroformylation Catalyst $HCo(CO)_3$

Tom Ziegler,*,† Luigi Cavallo,‡ and Attila Bérces†

Departments of Chemistry, University of Calgary, Calgary, Alberta, Canada T2N 1N4, and University of Naples, Naples, Italy

Received March 24, 1993®

A theoretical study has been carried out on the electronic and molecular structure of the hydroformylation catalyst $HCo(CO)_3$ as well as the parent molecule $HCo(CO)_4$. The study was based on a nonlocal density functional (DF) method. The parent molecule has a trigonal-bipyramidal structure with hydrogen in the axial position. The catalyst $HCo(CO)_3$ adopts a singlet ground state with a geometry of C_s symmetry where one equatorial CO group has been removed from $HCo(CO)_4$. The other singlet structure of C_{3v} symmetry with an axial CO group removed from $HCo(CO)_4$ is 35 kJ mol^{-1} higher in energy. Optimizations have further been carried out on five triplet states of $HCo(CO)_3$; they are found to be ~100 kJ mol^{-1} higher in energy than the C_s singlet structure. Calculations have also been carried out on the IR spectra of $HCo(CO)_4$ and $HCo(CO)_3$, in order to interpret the low-temperature vibrational spectra obtained in a krypton matrix after photolysis of $HCo(CO)_4$. The following bond energies have been obtained for $HCo(CO)_4$: $D_e(Co-CO_{ax})$ = 207 kJ mol^{-1}, $D_e(Co-CO_{eq})$ = 169 kJ mol^{-1}, and $D_e(Co-H)$ = 288 kJ mol^{-1}.

1. Introduction

The conversion of olefins and synthesis gas into aldehydes by the oxo or hydroformylation reaction is one of the few processes in which homogeneous catalysts are employed on an industrial scale. The most commonly used (pre)catalyst is $HCo(CO)_4$, which is generated *in situ* from the hydrogenation of $Co_2(CO)_8$ by H_2. However, (pre)catalysts derived from $HCo(CO)_4$ by replacing one or more CO groups with phosphines, or cobalt with rhodium, have also been employed.[1]

Heck and Breslow[2] suggested in 1962 that $HCo(CO)_3$ is the active catalyst in the hydroformylation reaction, and this suggestion has since prompted many attempts to identify and characterize this coordinatively unsaturated and highly reactive species. Photolysis[3] of the (pre)catalyst $HCo(CO)_4$ in inert-gas matrices have revealed several new IR bands, and these bands have been attributed to $HCo(CO)_3$ as well as other species. However, the interpretation of the new IR bands is not simple, and it is difficult to obtain any conclusive information about the structure of $HCo(CO)_3$.

There have been several early theoretical studies on the hydroformylation process[4,5] in general and the catalyst $HCo(CO)_3$ in particular. The first comprehensive[6a,b] theoretical investigation on $HCo(CO)_3$ was based on the *ab initio* HF method and concluded that $HCo(CO)_3$ had a triplet ground state. More recent *ab initio* studies at a higher level of theory find, on the other hand, a singlet ground state.[6c,7] Unfortunately, the higher level *ab initio* studies are hampered by the lack of full geometry optimization. We have previously studied[5a] $HCo(CO)_3$ in a theoretical treatment based on approximate density functional theory[8] (DFT). Our study was restricted to singlet states and based on the simplest level of DFT represented by the Hartree-Fock-Slater method[8] (HFS).

The uncertainty that still surrounds the electronic and molecular structure of $HCo(CO)_3$, in spite of its status as one of the most successful catalysts, has led us to conduct a comprehensive investigation of $HCo(CO)_3$ based on a more recent DFT scheme. We shall here report fully optimized singlet and triplet structures for various conformations and evaluate their relative energies. We shall further present calculated vibrational spectra for some of the more stable $HCo(CO)_3$ species and reconcile our calculations with the observed IR bands attributed to $HCo(CO)_3$.

2. Computational Details

The reported calculations were all carried out by utilizing the AMOL program system developed by Baerends et al.[9,10] and vectorized by Ravenek.[10b] The numerical integration procedure applied to the calculations was developed by te Velde and

† University of Calgary.
‡ University of Naples.
® Abstract published in *Advance ACS Abstracts*, August 15, 1993.

(1) (a) Pino, P.; Piacenti, F.; Bianchi, M. In *Orgnic Synthesis via Metal Carbonyls*; Wender, I., Pino, P., Eds.; Wiley: New York, 1977; Vol. II, pp 43-135. (b) Orchin, M.; Rupilius, W. *Catal. Rev.* **1972**, *6*, 85. (c) Orchin, M. *Acc. Chem. Res.* **1981**, *14*, 259.

(2) Heck, R. F.; Breslow, D. S. *J. Am. Chem. Soc.* **1961**, *83*, 4023.

(3) (a) Wermer, P.; Ault, B. S.; Orchin, M. *J. Organomet. Chem.* **1978**, *162*, 189. (b) Sweany, R. L.; Russell, F. N. *Organometallics* **1988**, *7*, 719.

(4) (a) Bellagamba, V.; Ercoli, R.; Gamba, A.; Suffritti, G. B. *J. Organomet. Chem.* **1980**, *190*, 381. (b) Grima, J. P.; Choplin, F.; Kaufmann, G. *J. Organomet. Chem.* **1977**, *129*, 221. (c) Fonnesbech, N.; Hjorkjaer, J.; Johansen, H. *Int. J. Quantum Chem.* **1977**, *12*, 95. (d) Fonnesbech, N. Ph.D. Thesis, Technical University of Denmark, 1979. (e) Pensak, D. A.; McKinney, R. J. *Inorg. Chem.* **1979**, *18*, 3407. (f) Eyermann, C. J.; Chung-Phillips, A. *J. Am. Chem. Soc.* **1984**, *106*, 7437.

(5) (a) Versluis, L.; Ziegler, T.; Baerends, E. J.; Ravenek, W. *J. Am. Chem. Soc.* **1989**, *111*, 2018. (b) Versluis, L.; Ziegler, T. *Organometallics* **1990**, *9*, 2985. (c) Versluis, L.; Ziegler, T. *Inorg. Chem.* **1990**, *29*, 5340. (d) Versluis, L.; Ziegler, T. *J. Am. Chem. Soc.* **1990**, *112*, 2985. (e) Ziegler, T. *Pure Appl. Chem.* **1991**, *63*, 873. (f) Ziegler, T.; Versluis, L. *Adv. Chem. Res. Ser.* **1992**, *No. 230*, 75.

(6) (a) Antolovic, D.; Davidson, E. R. *J. Am. Chem. Soc.* **1987**, *109*, 5828. (b) Antolovic, D.; Davidson, E. R. *J. Am. Chem. Soc.* **1987**, *109*, 977. (c) Antolovic, D.; Davidson, E. R. *J. Chem. Phys.* **1988**, *88*, 4967.

(7) Veillard, A.; Daniel, C.; Rohmer, M.-M. *J. Phys. Chem.* **1990**, *94*, 5556.

(8) Ziegler, T. *Chem. Rev.* **1991**, *91*, 651.

(9) Baerends, E. J.; Ellis, D. E.; Ros, P. *Chem. Phys.* **1973**, *2*, 41.

(10) (a) Baerends, E. J. Ph.D. Thesis, Vrije Universiteit Amsterdam, 1975. (b) Ravenek, W. In *Algorithms and Applications on Vector and Parallel Computers*; te Riele, H. J. J., Dekker, T. J., van de Vorst, H. A., Eds.; Elsevier: Amsterdam, 1987.

0276-7333/93/2312-3586$04.00/0

Baerends.[11] The geometry optimization procedure was based on the method introduced by Versluis[12] and Ziegler. Vibrational frequencies were evaluated from force constants calculated by numerical differentiation of the energy gradients.[13] An uncontracted triple-ζ STO basis set[14] was employed for the 3s, 3p, 3d, 4s, and 4p orbitals of cobalt, whereas 2s and 2p on carbon and oxygen, as well as 1s on hydrogen, were represented by a double-ζ STO basis set.[14] The ligand basis was augmented by a single STO polarization function, 2p on H and 3d on C and O. The other shells of lower energy was considered as core and frozen according to the method of Baerends et al.[9] In order to describe accurately the Coulomb and exchange potentials, extensive fits[15] of the density were carried out using a set of fit functions including s-, p-, d-, f-, and g-type functions.

Energies and structures in this study were based on the energy expression from the local density approximation[8] (LDA) augmented by nonlocal corrections to exchange[16a] and correlation.[16b] We shall refer to this method as the LDA/NL scheme. We have implemented the LDA/NL scheme self-consistently[17] in calculations on molecular structures,[18] force fields,[19] and transition states.[20] The vibrational frequencies will be calculated by the LDA method.

LDA/NL calculations of metal carbonyls,[21] binuclear metal complexes,[22] and alkyl and hydride complexes,[23] as well as complexes containing M–L bonds for a number of different ligands,[24] have shown that the approximate density functional method employed here affords metal–ligand and metal–metal bond energies of nearly chemical accuracy (± 5 kcal mol^{-1}). More than 50 molecular structures optimized by approximate density functional theory have been compared with experiment.[8] The agreement between experiment and theory is in most cases excellent. The application of approximate density functional theory to organometallic chemistry has been reviewed recently.[5,8,25]

3. Molecular and Electronic Structures of $HCo(CO)_4$ and $HCo(CO)_3$

We shall in the following discuss the molecular and electronic structure of $HCo(CO)_3$ after a few initial comments about the precursor $HCo(CO)_4$.

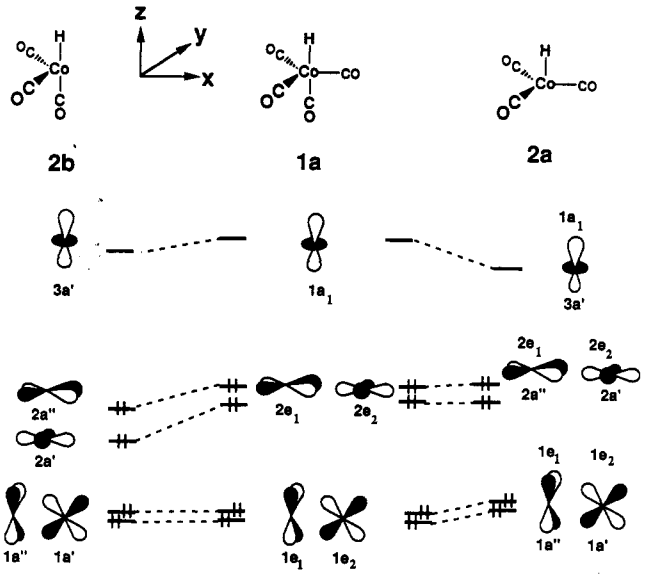

Figure 1. Diagram correlating orbitals of $HCo(CO)_4$ for conformation **1a** with orbitals of $HCo(CO)_3$ in the two singlet states **2a** and **2b**.

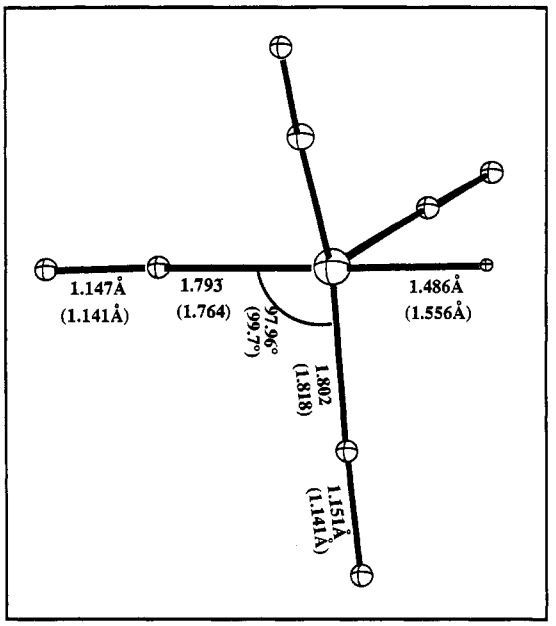

Figure 2. Optimized molecular structure of $HCo(CO)_4$ in conformation **1a**. Experimental values are given in parentheses.

$HCo(CO)_4$. Figure 1 affords a diagram in which the upper valence orbitals of $HCo(CO)_4$ and $HCo(CO)_3$ are correlated for the singlet states. The optimized ground-state geometry of $HCo(CO)_4$ has, according to experiment, a trigonal-bipyramidal C_{3v} structure (**1a**), with the hydride

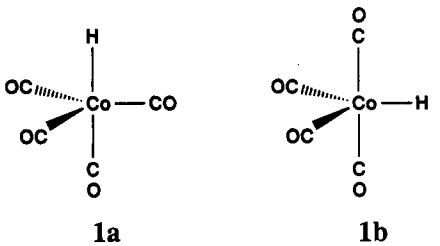

in an axial position (Figure 2) and a singlet electronic configuration given by $^1A_1[(1e)^4(2e)^4]$. The isomer with

(11) te Velde, G.; Baerends, E. J. *J. Comput. Phys.* **1992**, *99*, 84.
(12) Versluis, L.; Ziegler, T. *J. Chem. Phys.* **1988**, *88*, 322.
(13) Fan, L.; Versluis, L.; Ziegler, T.; Baerends, E. J.; Eavenek, W. *Int. J. Quantum. Chem., Quantum Chem. Symp.* **1988**, *S22*, 173.
(14) (a) Snijders, J. G.; Vernooijs, P.; Baerends, E. J. *At. Data Nucl. Data Tables* **1981**, *26*, 483–509. (b) Vernooijs, P.; Snijders, G. J.; Baerends, E. J. *Slater Type Basis Functions for the Whole Periodic System*; Internal Report; Free University, Amsterdam, The Netherlands, 1981.
(15) Krijn, J.; Baerends, E. J. *Fit Functions for the HFS-Method*; Internal Report (in Dutch); Free University, Amsterdam, The Netherlands, 1984.
(16) (a) Becke, A. D. *Phys. Rev.* **1988**, *A38*, 2398. (b) Perdew, J. P. *Phys. Rev.* **1986**, *B33*, 8822; **1986**, *B34*, 7046.
(17) Fan, L.; Ziegler, T. *J. Chem. Phys.* **1991**, *94*, 6057.
(18) Fan, L.; Ziegler, T. *J. Chem. Phys.* **1991**, *95*, 7401.
(19) (a) Fan, L.; Ziegler, T. *J. Chem. Phys.* **1992**, *96*, 9005. (b) Fan, L.; Ziegler, T. *J. Phys. Chem.* **1992**, *96*, 6937.
(20) Fan, L.; Ziegler, T. *J. Am. Chem. Soc.* **1992**, *114*, 10890.
(21) Ziegler, T.; Tschinke, V.; Ursenbach, C. *J. Am. Chem. Soc.* **1987**, *109*, 4825.
(22) Ziegler, T.; Tschinke, V.; Becke, A. *Polyhedron* **1987**, *6*, 685.
(23) (a) Ziegler, T.; Tschinke, V.; Becke, A. *J. Am. Chem. Soc.* **1987**, *109*, 1351. (b) Ziegler, T.; Cheng, W.; Baerends, E. J.; Ravenek, W. *Inorg. Chem.* **1988**, *27*, 3458. (c) Ziegler, T.; Tschinke, V.; Baerends, E. J.; Snijdes, J. G.; Ravenek, W. *J. Phys. Chem.* **1989**, *93*, 3050.
(24) (a) Versluis, L.; Ziegler, T. *Organometallics* **1990**, *9*, 2985. (b) Versluis, L.; Ziegler, T. *J. Am. Chem. Soc.* **1990**, *112*, 6763. (c) Harrod, J. F.; Ziegler, T.; Tschinke, V. *Organometallics* **1990**, *9*, 89. (d) Ziegler, T.; Fan, L.; Tschinke, V.; Becke, A. *J. Am. Chem. Soc.* **1989**, *111*, 2018. (e) Ball, J.; Boormann, M.; Ziegler, T. *J. Chem. Soc., Chem. Commun.* **1989**, 722. (f) Chivers, T.; Dhathathreyan, K. S.; Ziegler, T. *J. Chem. Soc., Chem. Commun.* **1989**, 86. (g) Masters, A. P. S.; Sorensen, T. S.; Ziegler, T. *Organometallics* **1989**, *8*, 1088.
(25) (a) Ziegler, T.; Tschinke, V. ACS *Symp. Ser.* **1990**, *No. 428*, 277. (b) Ziegler, T.; Snijders, J. G.; Baerends, E. J. *ACS Symp. Ser.* **1989**, *No. 383*, 322. (c) Ziegler, T.; Tschinke, V.; Versluis, L. *NATO ASI Ser.* **1986**, *C176*, 189. (d) Ziegler, T. *Pure Appl. Chem.* **1991**, *63*, 873. (e) Ziegler, T. *NATO ASI Ser.* **1992**, *C367*, 357. (f) Ziegler, T.; Versluis, L. *Adv. Chem. Ser.* **1992**, *230*, 75.

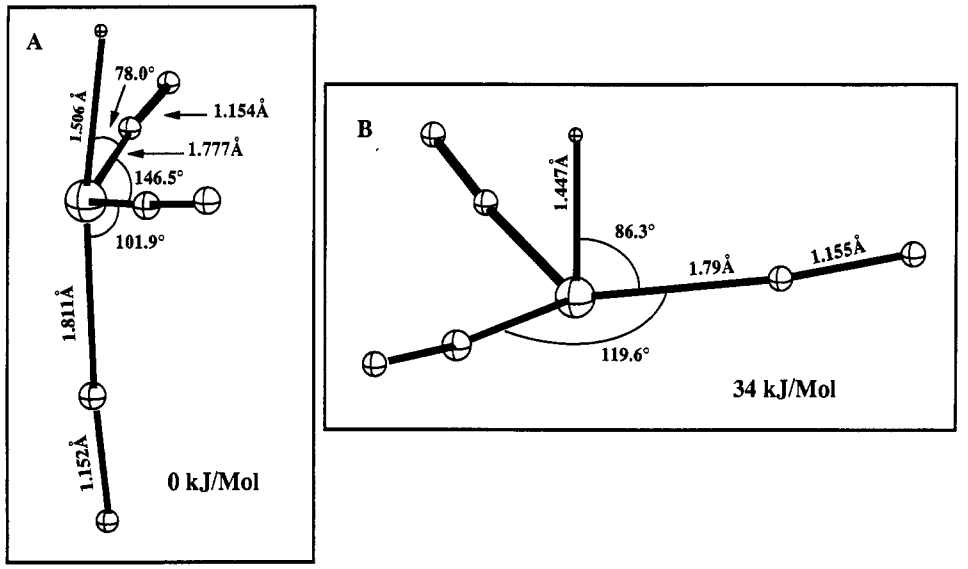

Figure 3. Optimized molecular structures of $HCo(CO)_3$ in the singlet state: (A) C_s structure **2b**; (B) C_{3v} structure **2a**. Energies are relative to **2b**.

a hydride in the equatorial position, **1b**, was calculated to be 58 kJ/mol higher in energy. We have previously studied[5a] the geometries and relative energies of **1a** and **1b** within the simpler DFT-based Hartree–Fock–Slater method. In that study **1a** was favored over **1b** by 63 kJ/mol. Figure 2 compares the calculated LDA/NL geometry with experimental results (in parentheses). We[18] have recently compared LDA/NL geometries with experiment for a number of organometallics and found an average deviation of 0.02 Å for M–L bond distances. The only M–L distance with a deviation larger than 0.03 Å was found for the Co–H bond, where the distance is underestimated by 0.07 Å (Figure 2). This deviation is surprising and cannot completely be explained by the fact that experimental[26] M–H distances are associated with uncertainties larger than for other metal–ligand bonds.

The first theoretical study on the relative stability of **1a** and **1b** was carried out by Antolovic and Davidson[6b] within the Hartree–Fock *ab initio* approach. Antolovic and Davidson[6b] performed a full geometry optimization on **1a** and **1b** and found **1b** to be more stable than **1a** by 4 kJ/mol. A subsequent CI calculation[6c] based on the Hartree–Fock geometries[6b] gave **1a** to be more stable than **1b** by 2 kJ/mol. Both results would indicate that **1a** as well as **1b** can be isolated, in disagreement with experiment, where only **1a** is observed. Antolovic and Davidson have suggested that this discrepancy primarily can be attributed to the poor Hartree–Fock geometries[6b] with Co–CO and Co–H distances up to 0.2 Å longer than those observed experimentally for **1a**. In fact, this notion has been confirmed by Veillard[7] et al. in calculations where only the angular degrees of freedom were optimized, whereas the Co–CO and Co–H distances were fixed at "experimental" values. The Hartree–Fock method now favors **1a** by 29 kJ/mol, and this value is increased to 63 kJ/mol when electron correlation (CASSCF) is included. Thus, the constrained geometry approach in conjunction with CASSCF affords the same results for the relative energies of **1a** and **1b** as the DFT-based methods[5a] with full optimization.

Molecular Structure of $HCo(CO)_3$ at the Singlet Surface. One can imagine the two basic structures **2a** and **2b** for $HCo(CO)_3$, corresponding to the removal of, respectively, an axial and equatorial CO ligand from **1a**.

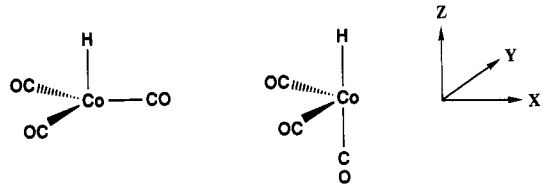

2a **2b**

An optimization of **2a** and **2b** on the singlet surface afforded the two structures given in parts B and A of Figures 3, respectively. The structure in Figure 3B has C_{3v} symmetry and an electronic configuration given by $^1A_1[1e)^4(2e)^4]$ (see Figure 1), whereas the structure in Figure 3A has C_s symmetry with the electronic configuration $^1A[(1a')^2(2a')^2(1a'')^2(2a'')^2]$ (Figure 2). The geometry optimizations were carried out at the LDA/NL level of theory, and we find from the LDA/NL energy expression that the C_s geometry is 35 kJ/mol more stable than the C_{3v} structure. A previous study based on the HFS method gave the corresponding difference as 38 kJ/mol. Thus, the inclusion of nonlocal corrections has only a marginal influence on the relative stability of the two structures in Figure 3.

The C_{3v} structure has a shorter Co–H distance than in $HCo(CO)_4$, since the axial trans carbonyl is missing. The most notable feature of the C_s structure is the expected[5a] increase in the equatorial CO–Co–CO angle from 120 to 146°. The increase will reduce the antibonding interaction between the d_{xy} orbital on cobalt and the σ_{CO} orbitals on the two equatorial CO ligands.

The calculations on **1a**, **2a**, and **2b** allow us to evaluate the first dissociation energy of an axial CO ligand in $HCo(CO)_4$ as 206.8 kJ/mol, whereas the corresponding equatorial dissociation energy is 169.3 kJ/mol. It is thus understandable that high temperatures are required to generate a sufficient concentration of $HCo(CO)_3$ from the precatalyst $HCo(CO)_4$. The dissociation of the Co–H bond requires by comparison 288 kJ/mol according to a similar LDA/NL calculation.[27]

(26) McNeil, E. A.; Scholer, F. R. *J. Am. Chem. Soc.* **1977**, *99*, 6243.

There have been two *ab initio* studies on the singlet states of $HCo(CO)_3$. Antolovic and Davidson[6a,b] found from HF calculations with full geometry optimization that the C_{3v} structure **2a** was more stable than the C_s structure **2b** by 13 kJ/mol. The calculated Co–H and Co–CO_{eq} distances were further found to be substantially different in the two structures.

Veillard[7] et al. have also studied the relative stability of the two singlet states in Figure 3. The Co–H, Co–CO_{ax}, and Co–CO_{eq} distances were fixed and taken from the experimental structure of $HCo(CO)_4$. For the C_{3v} structure the single angular degree of freedom was optimized, whereas the angular geometrical parameters for the C_s structure were taken from the previous Hartree–Fock study[6] by Antolovic and Davidson. Veillard[7] et al. find **2a** to be favored by 8 kJ/mol at the HF level and 40 kJ/mol at the CASSCF level of theory. This is in contrast to our LDA/NL study, in which **2b** is favored by 35 kJ/mol.

We feel that the present investigation presents the most complete theoretical study on the singlet structures of $HCo(CO)_3$. Further assessments based on *ab initio* methods must await CASSCF–CI calculations with full geometry optimization. We have previously demonstrated that the LDA/NL method provides accurate estimates of structures[19] and energy differences[8] for organometallics. Further, it has recently been shown[28] that the LDA/NL scheme estimates bond energies with the same accuracy as the G1 *ab initio* method of Pople[29] et al. for the G1 thermochemical data base[28] of organic molecules. We shall shortly reconcile our findings with the few available experimental data for $HCo(CO)_3$.

Molecular Structure of $HCo(CO)_3$ at the Triplet Surface. Antolovic and Davidson[6a,b] have also explored the triplet surface of $HCo(CO)_3$. A full optimization on the HF level revealed several triplet states, all of which were of lower energy than the two singlet structures **2a** and **2b**. A later investigation[6c] based on CI with geometries adopted from the HF calculations[6a,b] found the singlet to be the most stable. Veillard[7] et al. have carried out CASSCF calculations on the triplet surface of $HCo(CO)_3$ with bond distances taken from the experimental structure of $HCo(CO)_4$ and bond angles from the HF geometries of Antolovic and Davidson.[6c] Veillard[7] et al. find in this study that the singlet states are most stable.

Our previous HFS examination[5a] of $HCo(CO)_3$ was restricted to the singlet surface, and we shall here extend the present study to include triplets as well. Our discussion will focus on the geometrical aspects, since a determination of triplet structures on a higher level of theory than the Hartree–Fock method is missing. We have located a total of five triplet states, of which three originate from the C_{3v} singlet structure **2a** and two from the C_s singlet structure **2b**.

The three triplet structures originating from **2a** are displayed in Figure 4. Their relation to the singlet geometry, **2a**, is illustrated in the correlation diagram of Figure 5. A promotion of an electron from each of the 2e orbitals to $1a_1$ gives rise to the $^3A_2[(2e_1)^1(2e_2)^1(1a_1)^2]$ state **3a** (Figure 5), for which the optimized structure is shown in Figure 4A. The most significant feature of **3a** (Figure 4A) compared to the parent structure **2a** (Figure 3A) is an increase in the H–Co–CO_{eq} angle from 82 to 115°. This increase reduces the antibonding interaction between d_{z^2} and the equatorial σ_{CO} orbitals and allows in addition the $4p_z$ orbital to mix in so as to reduce the antibonding interaction between d_{z^2} and $1s_H$ by polarizing the metal hydride away from the hydride. The $^3A_2[(2e_1)^1(2e_2)^1(1a_1)^2]$ state **3a** is 130 kJ/mol above **2b** in energy.

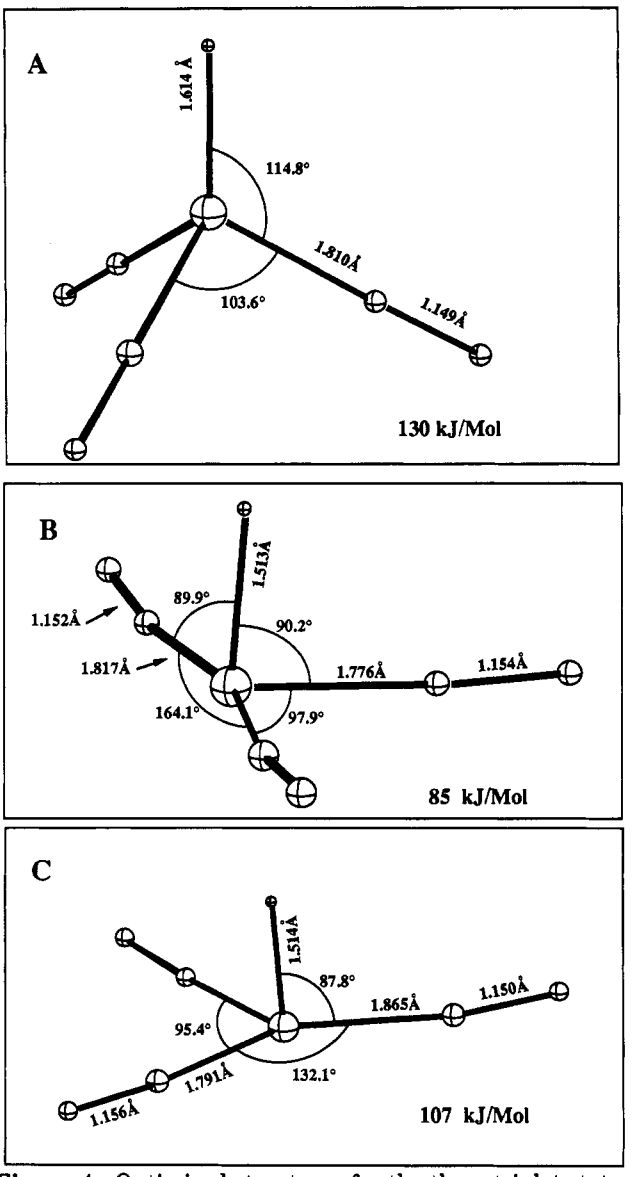

Figure 4. Optimized structures for the three triplet states of $HCo(CO)_3$ originating from **2a**: (A) $^3A_2[(2e_1)^1(2e_2)^1(1a_1)^2]$; (B) $^3A''[(2a')^2(2a'')^1(3a')^1]$; (C) $^3A'[(2a')^1(2a'')^2(3a')^1]$. Energies are relative to **2b**.

The promotion of an electron from $2e_2$ to $1a_1$ results in the $^3E_2[(2e_1)^2(2e_2)^1(1a_1)^1]$ state which can undergo distortion to produce the $^3A''[(2a')^2(2a'')^1(3a')^1]$ state **3b** of C_s symmetry (Figure 5). The distortion involves an increase in one of the trigonal CO_{eq}–Co–CO_{eq} angles from 120 to 164° (Figure 4B). This distortion will stabilize the doubly occupied 2a′ ($2e_1$) orbital and raise the energy of the singly occupied 2a″ ($2e_2$) orbital, thus resulting in a total stabilization. The $^3A''[(2a')^2(2a'')^1(3a')^1]$ state **3b** of C_s symmetry is situated 85 kJ/mol above **2b**.

The promotion of an electron from $2e_1$ to $1a_1$ results in the $^3E_1[(2e_1)^1(2e_2)^2(1a_1)^1]$ state, which after distortion turns into **3c** of C_s symmetry with the electronic configuration

(27) Folga, E.; Ziegler, T. *J. Am. Chem. Soc.*, submitted for publication.
(28) Becke, A. D. *J. Chem. Phys.* **1992**, *96*, 2155.
(29) Pople, J. A.; Head-Gordon, M.; Fox, D. J.; Raghavachari, K.; Curtiss, L. A. *J. Chem. Phys.* **1989**, *90*, 5622.

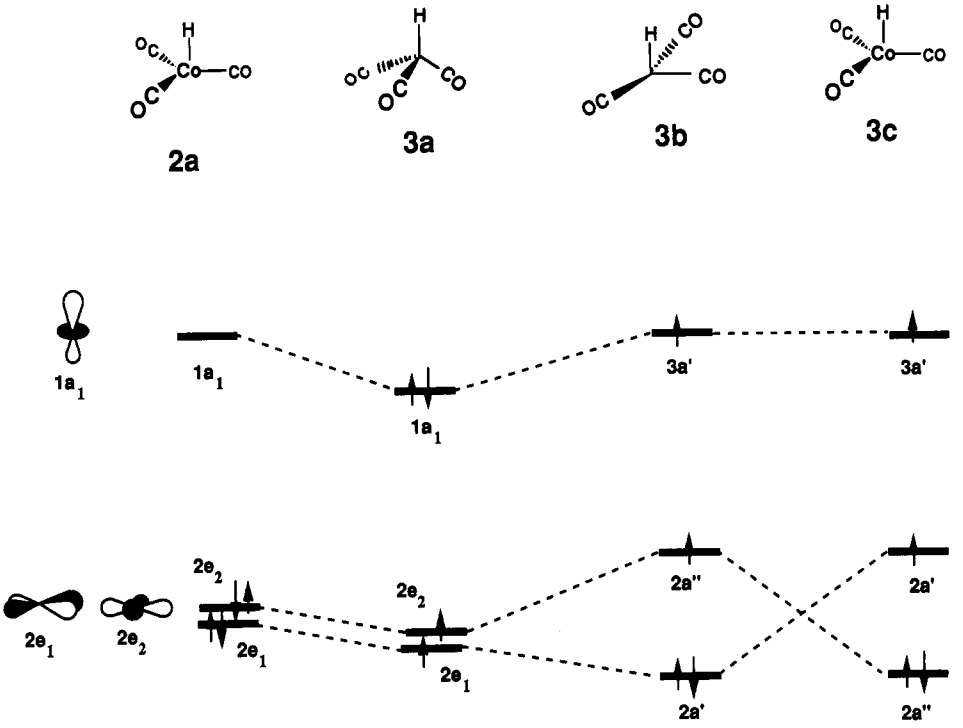

Figure 5. Diagram correlating orbital levels of singlet state **2a** with the three triplet states **3a**, **3b**, and **3c**.

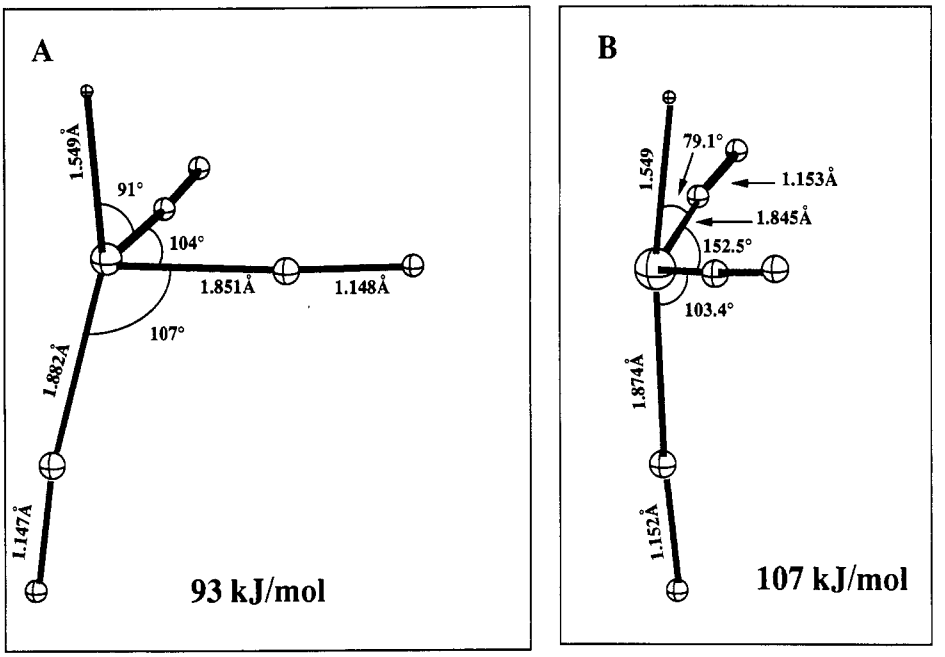

Figure 6. Molecular structures of the two triplet states originating from **2b**: (A) $^3A''[(2a')^2(2a'')^1(3a')^1]$; (B) $^3A'[(2a')^1(2a'')^2(3a')^1]$. Energies are relative to **2b**.

$^3A'[(2a')^1(2a'')^2(3a')^1]$ (Figure 5). The distortion involves in this case a decrease in one of the trigonal CO_{eq}–Co–CO_{eq} angles from 120 to 95° (Figure 4C). This distortion will stabilize the doubly occupied 2a″ ($2e_2$) orbital and raise the energy of the singly occupied 2a′ ($2e_1$) orbital, thus resulting in a total stabilization. The $^3A'[(2a')^1(2a'')^2(3a')^1]$ state **3c** of C_s symmetry is situated 107 kJ/mol above **2b**.

There are two triplet states originating from the C_s singlet $^1A[(1a')^2(2a')^2(1a'')^2(2a'')^2]$ (**2b**). The structures of the two triplets are displayed in Figure 6, and their correlation to the singlet **2b** is illustrated in Figure 7. Promotion of an electron from 2a″ to 3a′ results in the $^3A''[(1a')^2(2a')^2(1a'')^2(2a'')^1(3a')^1]$ state **4a** (Figure 7), with the structure shown in Figure 6A. The energy of **4a** is 93 kJ/mol above the **2b** singlet ground state. The most characteristic feature of **4a** is a decrease in the CO_{eq}–Co–CO_{eq} angle from 146° in **2b** to 104° in **4a**. The distortion is similar to that observed for the $^3A'[(2a')^1(2a'')^2(3a')^1]$ state **3c** (Figure 4C) and can be rationalized in a similar manner. The promotion of an electron from 2a′ to 3a′ results in the $^3A'[(1a')^2(2a')^1(1a'')^2(2a'')^2(3a')^1]$ state **4b** (Figure 7), with the structure shown in Figure 6B. The energy of **4b** is 107 kJ/mol above the **2b** singlet ground state. The CO_{eq}–Co–CO_{eq} angle is now increased from 146° in **2b** to 151° in **4b**. The increase follows the trend calculated for the $^3A''[(2a')^2(2a'')^1(3a')^1]$ state **3b** of C_s symmetry (Figure 4B).

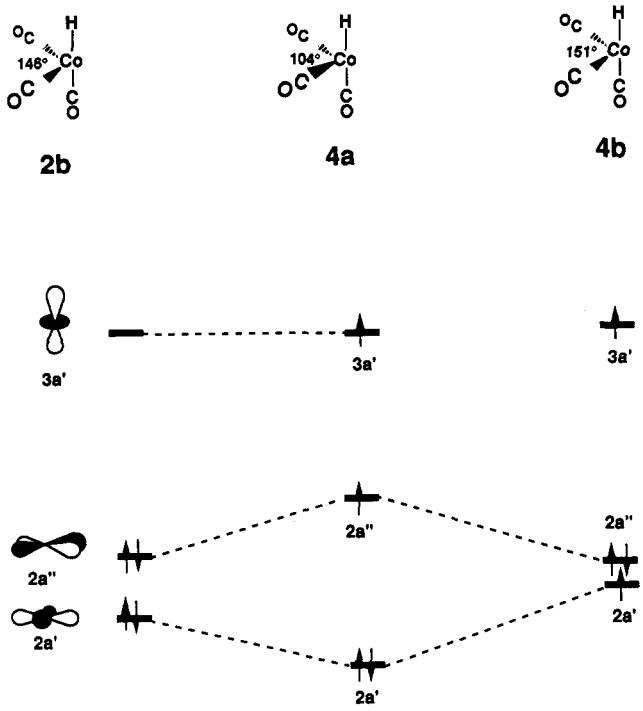

Figure 7. Diagram correlating orbital levels of singlet state **2b** with the two triplet states **4a** and **4b**.

4. Vibrational Spectra of $HCo(CO)_4$ and $HCo(CO)_3$

It follows from the previous discussion that the present DFT study points to the C_s structure **2b** of $HCo(CO)_3$ as more stable than conformation **2a** with C_{3v} symmetry. However, the energy difference of 35 kJ/mol does not rule out the coexistence of both conformations, especially since $HCo(CO)_3$ is generated by high-energy pathways involving photolysis of $HCo(CO)_4$. Very few experimental techniques exist that can detect such highly reactive and short-lived species. One of these techniques is the isolation of $HCo(CO)_3$ within a matrix of inert gas. Attempts can then be made to characterize the trapped species by spectroscopic studies. In the case of $HCo(CO)_3$, use has been made of vibrational spectroscopy,[3] and we shall in the following discuss the IR spectra of $HCo(CO)_4$ and $HCo(CO)_3$.

$HCo(CO)_4$. The first infrared investigation of $HCo(CO)_4$ by Edgell et al.[30a] interpreted the most important features of the spectrum, which has served as a basis for further studies since. Other studies[3a,b] were concerned with the photolysis of $HCo(CO)_4$, while a recent Fourier transform IR study investigated the Co–H and CO stretches in different matrix materials and fluid media.[30b] The observed frequencies for the CO and Co–H stretching region are displayed in Table I. The listed experimental frequencies are those for the Ar matrix by FTIR measurements.[30b]

We have carried out LDA calculations on the vibrational spectrum of $HCo(CO)_4$ by evaluating force constants, atomic polar tensors, frequencies, and normal modes of $HCo(CO)_4$. Our calculated Co–H bond length is somewhat shorter then the experimental bond length for $HCo(CO)_4$; therefore, we expect the corresponding predicted force constant and frequency to be too high. For this reason, in our direct quantum-mechanical calculation, the Co–H frequency appeared in the CO stretching region, resulting in an artificial strong mixing of the a_1 symmetry CO and Co–H stretching modes. Consequently, we had to introduce a scaling factor, to correct for this deficiency. In the scaling process, we follow the procedure introduced by Pulay and co-workers.[31] After the Co–H stretching force constant was scaled down by an optimized scaling factor of 0.876, the CO stretching region of the spectrum matched very well with the experimentally observed spectra for $HCo(CO)_4$ and $DCo(CO)_4$, the theoretical frequencies being systematically too high by about 30 cm^{-1}. Another scaling factor was introduced for the CO stretching force constants; its optimized value is 0.960. With the help of these two empirical constants, we were able to reproduce the Co–H and CO stretching region of the spectrum (seven frequencies) with an average error of 4.2 cm^{-1}. Since the error in the quantum-mechanical calculation is systematic, these scaling factors can also be used to correct for the error in the force constants of $HCo(CO)_3$. The observed frequencies of $HCo(CO)_4$ vary in different matrices. When determining the scaling factors, we have chosen the experimental frequencies from the Ar matrix experiment, since we compare the spectrum of $HCo(CO)_3$ also in an Ar matrix. Further, this measurement was taken by an accurate FTIR instrument. Note that the choice of other experimental frequencies would have led to somewhat different frequencies but the same conclusion.

The theoretical CO and Co–H stretching frequencies are presented in Table I along with calculated intensities. The scaled harmonic force field constants are given in Table II. We note that the CO stretching force constants are larger for CO_{eq} than for CO_{ax} in the case of $HCo(CO)_4$ with conformation **1a**. This is related to the fact that CO_{eq} can receive density from two sets of fully occupied d orbitals, whereas only one set is available for CO_{ax}. The CO_{eq} and CO_{ax} constants are further seen to be reduced

Table I. Scaled Quantum-Mechanical Force Field Predictions of Frequencies and Intensities for $HCo(CO)_4$

$HCo(CO)_4$				$DCo(CO)_4$	
calcd[a]	exptl[b,c]	sym	potential energy distribn and/or descripn	calcd[a]	exptl[d]
2115 (169)	2121(1)	a_1	0.36 CO_{ax}; 0.18 CO_{eq}; 0.18 CO_{eq2}; 0.18 CO_{eq3}	2112	2121
2060 (369)	2058 (23.4)	a_1	0.52 CO_{ax}; 0.13 CO_{eq1}; 0.13 CO_{eq2}; 0.13 CO_{eq3}; 0.07 CoH	2052	2053
2040 (242)	2034 (79.4)	e	degenerate eq CO stretches	2038	2034
1966 (79)	1966	a_1	0.92 CoH; 0.09 CO_{ax}	1406	

[a] Frequencies in cm^{-1} and intensities in km mol^{-1} in parentheses. [b] Frequencies from ref 30b. [c] Reference 3b, with relative intensities in parentheses. [d] Reference 3b.

Table II. Selected Scaled Harmonic Force Constants for $HCo(CO)_4$ and $HCo(CO)_3$[a]

	$HCo(CO)_4$	C_{3v} $HCo(CO)_3$	C_s $HCo(CO)_3$
Co–H	2.286	2.581	2.083
CO_{ax}	16.949		16.443
CO_{eq}	16.692	16.445	16.537
CO_{eq2}–CO_{eq3}	0.163	0.214	0.145
CO_{eq}–CO_{ax}	0.201		0.219
CoH–CO_{eq3}	–0.016	–0.032	–0.022
CoH–CO_{ax}	–0.016		–0.032

[a] Units are mdyn/Å.

(30) (a) Edgell, W. F.; Magee, C.; Gallup, G. *J. Am. Chem. Soc.* **1956**, *78*, 4185. (b) Kritjánsdóttir, S. S.; Norton, J. R.; Moroz, A.; Sweany, R. L.; Whittenburg, S. L. *Organometallics* **1991**, *10*, 2357.

(31) Pulay, P.; Fogarasi, G.; Pongor, G.; Boggs, J. E.; Vargha, A. *J. Am. Chem. Soc.* **1983**, *105*, 7037.

Table III. Scaled Quantum-Mechanical Force Field Predictions of Frequencies and Intensities for the C_{3v} Conformer of $HCo(CO)_3$[a]

C_{3v} $HCo(CO)_3$	sym	potential energy distribn and/or descripn	deuterated
2103 (8)	a_1	0.96 CoH; 0.01 CO_{eq1}; 0.01 CO_{eq2}; 0.01 CO_{eq3}	1500
2086 (50)	a_1	symmetric eq CO stretch (CoH)	2086
2017 (1288)	e	degenerate eq CO stretch	2017
478 (29)	a_1	sym CoC_{eq} stretch	478

[a] Frequencies in cm^{-1} and intensities in km mol^{-1}, in parentheses.

in $HCo(CO)_3$, where the back-donation is spread over fewer CO ligands.

We find the totally symmetric CO mode of a_1 symmetry at 2115 cm^{-1}. This mode has the axial and equatorial CO stretches in phase. The corresponding out-of-phase combination, also of a_1 symmetry, is found at 2060 cm^{-1}. The degenerate e mode at 2040 cm^{-1} corresponds to the equatorial CO stretches, whereas the band at 1966 cm^{-1} represents the Co–H stretch.

Also shown in Table I are the calcualted absolute intensities as well as the experimental relative intensities for $HCo(CO)_4$. Previous experience[32] with intensity calculations has shown that the DF-based methods predict the CO stretching intensities to be too high; however, the relative magnitudes are usually correct. In our prediction for the parent molecule, the band at 2058 cm^{-1} is more intense than the band at 2034 cm^{-1}, as opposed to the experimentally observed intensities.

$HCo(CO)_3$. Wermer et al.[3a] were the first to identify the reactive and coordinatively unsaturated hydroformylation catalyst $HCo(CO)_3$. Their identification was based on the appearance and growth of IR bands at 2018 and 2025 cm^{-1} on irradiation of $HCo(CO)_4$ in a low-temperature argon matrix. When substantial amounts of CO were present in the Ar matrix, these bands failed to appear after irradiation. Further, the presence of ethylene and propylene in the matrix inhibited the growth of this set of bands. This study assumes a C_{3v} structure of $HCo(CO)_3$. The findings by Wermer et al.[3a] have since been confirmed by Sweany and Russel[3b] in a photolysis experiment involving $HCo(CO)_4$ in an H_2 matrix.

The calculated frequencies for the C_{3v} conformation (**2a**) of $HCo(CO)_3$ are given in Table III. The Co–H stretch is now found above the CO frequencies at 2103 cm^{-1}. The relatively high Co–H frequency reflects an increase in the Co–H bond strength compared to the parent molecule $HCo(CO)_4$, as discussed previously. The CO stretches are calculated to be at 2086 cm^{-1} for the symmetrical a_1 mode and at 2017 cm^{-1} for the e modes. A high intensity is further seen to be associated with the e mode (Table III).

The calculated frequencies for the C_s structure (**2b**) of $HCo(CO)_3$ are given in Table IV. For this conformation of the Co–H stretch is at a lower frequency than the CO stretches. We find the totally symmetric CO mode of a′ symmetry at 2104 cm^{-1}. This mode has the axial and equatorial CO stretches in phase. The corresponding out-of-phase combination, also of a′ symmetry, is found at 2033 cm^{-1}. We finally have the asymmetric equatorial CO stretching mode of a″ symmetry at 2022 cm^{-1}.

It is important to point out that the transfer of scaling factors is a less serious assumption than the direct transfer of force constants from $HCo(CO)_4$ to $HCo(CO)_3$. The

(32) (a) Fan, L.; Ziegler, T. *J. Chem. Phys.* **1992**, *96*, 9005. (b) Fan, L.; Ziegler, T. *J. Phys. Chem.* **1992**, *96*, 6937.

Table IV. Scaled Quantum-Mechanical Force Field Predictions of Frequencies and Intensities for the C_s Conformer of $HCo(CO)_3$[a]

C_s $HCo(CO)_3$	sym	potential energy distribn and/or descripn	deuterated
2104 (78)	a′	0.35 CO_{eq3}; 0.35 CO_{eq2}; 0.22 ax CO	2104
2033 (577)	a′	0.71 CO_{ax}; 0.12 CO_{eq2}; 0.12 CO_{eq3}	2127
2022 (380)	a″	0.50 CO_{eq3}; 0.50 CO_{eq2}	2121
1879 (40)	a′	0.96 Co–H; 0.05 ax CO	1342
488 (5)	a′	0.18 $CoCO_{eq2}$ bend; 0.18 $CoCO_{eq3}$ bend; 0.10 CoC_{ax}	

[a] Frequencies in cm^{-1} and intensities in km mol^{-1} in parentheses.

Co–H stretching force constants, for example, which are assumed to be the same in a previously used empirical force field,[3b] are 2.286, 2.581, and 2.083 mdyn/Å for **1a**, **2a**, and **2b**, respectively, on the basis of quantum-mechanical data (Table II). Also, it is well established that the error is systematic in the force constants of closely related molecules. Thus, the scaling factors obtained from $HCo(CO)_4$ should be accurate enough to predict the spectrum of the two possible conformations of $HCo(CO)_3$.

We calculate the C_{3v} conformation **2a** to have a single absorption band at 2017 cm^{-1} in the region where Wermer et al.[3a] observe the two frequencies attributed to $HCo(CO)_3$. The band at 2017 cm^{-1} is predicted to have a large intensity of 1288 km mol^{-1} (Table III). The absolute intensity and position of this band correlates very well with an intense band, reported independently by Wermer[3a] et al. and Sweany and Russel[3b] at 2018 and 2020 cm^{-1}, respectively. The very large absorption coefficient would indicate that this band should be observed, even if the concentration of the C_{3v} isomer is very small.

The C_s conformation **2b** is predicted to have two bands in the region for the two frequencies at 2018 and 2025 cm^{-1} observed by Wermer[3a] et al. (Table IV). We predict two strong bands; one at 2022 cm^{-1} corresponding to the a″ mode and another of a′ symmetry at 2033 cm^{-1}. The a″ band at 2022 cm^{-1} might coincide with the similar energy band of the other conformer **2a**, which explains the observed variation in the intensity ratios.[3] Also, the experimental band of this region has a shoulder, which has not been interpreted.[3b]

The predicted band at 2033 cm^{-1} might well correspond to the observed frequency at 2025 cm^{-1}. Wermer et al. explain the appearance of the 2025-cm^{-1} absorption as a result of a site splitting of the doubly degenerate 2018-cm^{-1} band of the C_{3v} conformation. In our opinion the site splitting would not explain the considerable difference in the intensities. We explain the observation of two bands with different intensity by the presence of the lower symmetry isomer of $HCo(CO)_3$ as well.

We also predict a less intense band at 2104 cm^{-1} due to the C_s conformation of $HCo(CO)_3$. This band does not shift on deuteration and correlates well with the experimentally observed band[3b] at 2100.2 cm^{-1}. Its intensity ratio with respect to the 2018-cm^{-1} band is essentially correct.

On the basis of our calculated frequencies and intensities we can also assign the experimentally[3a] observed peak at 485 cm^{-1}. We did not find any band of the parent molecule with considerable predicted intensity in this region. However, on the removal of the axial CO group, the symmetrical Co–C_{eq} stretching mode shifts from 469 to 478 cm^{-1} and significantly intensifies, with a predicted intensity of 29 km/mol. On the removal of an equatorial

CO group, the Co–C frequencies shift to higher wavenumbers, while a Co–C–O deformation mode is predicted at 488 cm^{-1}, with 5 km mol^{-1} intensity. The experimental band at 485 cm^{-1} most likely correlates to our 478-cm^{-1} intense band, since the low intensity of the 488-cm^{-1} band of the C_s isomer makes it unlikely to be detected in low quantities. This observation also supports the presence of the C_{3v} isomer.

Wermer et al. as well as Sweany and Russel observed a band around 1999 cm^{-1}. Wermer et al. assigned it to $HCo(CO)_3$, ^{13}CO, or an impurity. Neither of the two $HCo(CO)_3$ conformations is calculated to have an absorption in this region. Thus, it is not likely to be associated with $HCo(CO)_3$.

We conclude from the analysis given above that both conformations of $HCo(CO)_3$ are observed in the experimental study. Since the observed CO stretching band for the C_{3v} isomer has much larger absorption coefficient than most other CO bands, and this band probably coincides with a band of the C_s symmetry isomer, it is very difficult to speculate about the ratio of the two possible isomers.

5. Concluding Remarks

We have carried out nonlocal DF calculations on the electronic and molecular structure of $HCo(CO)_3$ as well as the parent molecule $HCo(CO)_4$. The calculations were carried out with full geometry optimization. The hydroformylation catalyst $HCo(CO)_3$ is predicted to have a singlet ground state with a geometry of C_s symmetry (**2b**). The corresponding singlet with a structure of C_{3v} geometry (**2a**) is higher in energy by 35 kJ mol^{-1}. The triplet states of lowest energy were found to be ~100 kJ mol^{-1} above **2b**.

Calculations have also been carried out on the IR spectra of $HCo(CO)_4$ and $HCo(CO)_3$, in order to interpret the low-temperature vibrational spectra obtained in a krypton matrix after photolysis of $HCo(CO)_4$. The calculations further support the suggestion[3a] that the two bands observed by Wermer et al.[3a] at 2018 and 2025 cm^{-1}, respectively,[1] originate from $HCo(CO)_3$. The DF calculations indicate in addition that the intense band at 2018 cm^{-1} can be attributed to either of the $HCo(CO)_3$ conformations (**2a** and **2b**), whereas the absorption at 2025 cm^{-1} most likely is due to the C_s conformer **2b**.

Acknowledgment. We thank the Natural Sciences and Engineering Research Council of Canada (NSERC) for financial support. All calculations were carried out at the IBM 6000 computer installations at the University of Calgary. L.C. gratefully acknowledges the "Instituto Guido Donegani, Novara, Italy", for financial support. We gratefully acknowledge the Donors of the Petroleum Research Fund, administered by the American Chemical Society (ACS-PRC No. 27023-AC3).

OM930183G